Geoscience Frontiers 15 (2024) 101655

Contents lists available at ScienceDirect

Geoscience Frontiers

journal homepage: www.elsevier.com/locate/gsf

Research Paper

Effect of geopolitical risk and economic uncertainty indices on renewable energy

Xin Zhao [a], Kamel Si Mohammed [b], Yaohui Wang [c,*], Paweł Stępień [d], Grzegorz Mentel [e]

[a] School of Statistics and Applied Mathematics, Anhui University of Finance and Economics, Bengbu, PR China
[b] Faculty of Economics and Management, University Ain Temouchent Belhadj Bouchaib, Algeria
[c] School of Urban and Regional Science, Institute of Finance and Economics Research, Shanghai University of Finance and Economic, Shanghai, PR China
[d] Institute of Economics and Finance, University of Szczecin, Poland
[e] Department of Quantitative Methods, Faculty of Management, Rzeszow University of Technology, Rzeszow 35-959, Poland

ARTICLE INFO

Article history:
Received 13 December 2022
Revised 14 February 2023
Accepted 20 June 2023
Available online 25 June 2023

Keywords:
Renewable energy
Uncertainty indices
Impulse response
Safe-haven

ABSTRACT

In this study, the relationships between five renewable energy sub-sectors markets and the geopolitical risk (GPR) and economic uncertainty indices (EUI) were examined using daily data from March 30, 2012, to April 1, 2022. Convergent cross mapping results show that the renewable energy indices have definite relationships with the GPR and EUI. The renewable energy indices show differences in response directions, speed and trends for a standard information difference impulse from the GPR and the EUI. A positive dynamic conditional correlation between renewable energies and EUI was observed in the first and second waves of the COVID-19 outbreak. In contrast, there was a relatively decreased effect for two risk indices during the Russia–Ukraine conflict of February–March 2022. Our results show that renewable energy may act as a time-varying hedge against economic uncertainty and GPR owing to its safe-haven properties at various scales. Moreover, building more secure and reliable renewable energy systems can help countries to increase their energy independence, which protects them against the risks of political and economic uncertainty.

1. Introduction

The past decade has included a number of significant geopolitical and economic events with global implications. These have included the Paris terror attacks (2015), military tensions between the USA and Iran (2020), and the Russia–Ukraine war (2014, 2022). In addition, oil, gas, and fossil fuel prices have been weaponized to put pressure on conflicted parties. The COVID-19 pandemic and its aftermath have had the most significant negative economic impact, having global economy and decreased the availability and economic viability of traditional energy supplies worldwide (Johnston, 2020; Kang et al., 2021). The Russia–Ukraine conflict has also brought concerns over energy security to the forefront, as searches for new energy sources commonly intensify when geopolitical risk rises. Over the same decade, there has been a global transition toward renewable energy, which is fundamentally different to fossil fuels and has the potential to facilitate geopolitical stability and international peace (Overland, 2019; Vakulchuk et al., 2020). To continue generating power in the face of rising fossil fuel cost and insecurity, governments have turned to gas, wind, and hydropower.

In light of these changes, studying the impacts of geopolitical and economic uncertainty on energy security has become critical. Numerous studies have analyzed the effects of geopolitical risk (GPR) and economic uncertainty indices (EUI) on variables such as GDP growth (Dibiasi et al., 2018; Xue et al., 2022), unemployment (Davidescu et al., 2021; Eksi and Tas, 2022), tourism (Tiwari et al., 2019; Gozgor et al., 2022), inflation (Azad and Serletis, 2021; Bai, 2021), financial markets (Alqahtani and Klein, 2021; Jiao et al., 2022), and commodity markets (Tiwari et al., 2021; Chen et al., 2022). Liu et al. (2022) investigated the spillover effects of economic uncertainty on renewable energy markets in the time–frequency domain. They found that the impact of EUI caused by COVID-19 was more significant than the impact of the financial crisis. Hemrit and Benlagha (2021) reported a significant positive effect of pandemic uncertainty on the WilderHill New Energy Global Innovation Index (NEX) which benchmarks renewable energy. Are et al. (2020) utilized the Diebold–Yilmaz (2014) approach to conclude that Brexit influenced clean energy

* Corresponding author.
E-mail address: wangyaohui97@163.com (Y. Wang).

https://doi.org/10.1016/j.gsf.2023.101655

enterprises represented on the New York Stock Exchange and the European Renewable Energy Index (IRIX). Ahmad et al. (2018) applied multivariate Generalized AutoRegressive Conditional Heteroskedasticity (GARCH) to demonstrate that the Volatility Index (VIX) is the most effective asset for portfolio hedging against clean energy equities. Dutta (2017) demonstrated that there was a more considerable effect on the oil price uncertainty (OVX) than the oil price spot on the clean energy equity market. Yahya et al. (2021) combined the Threshold Vector Error Correction Model and Dynamic Conditional Corelational Autoregressive Conditional Heteroscedasticity Model to examine volatility spillover between the clean energy index and oil prices during the EUI caused by COVID-19; they found only a weak correlation between oil prices and the alternative energy index prior to the EUI period, with a stronger correlation from after the financial crisis until the beginning of the COVID-19 pandemic. Ji et al. (2018) showed that there was a negative dependence between uncertainties and renewable energy markets.

Nevertheless, relatively fewer studies have considered the effects of geopolitical risk on renewable energy markets. Sweidan (2021) used quarterly data and the Autoregressive Distributed Lag model in the United States to document that geopolitical risk positively affects renewable energy consumption. However, Su et al. (2020) found no causality between GPR and renewable energy. Yang et al. (2021) found evidence of asymmetric risk spillover and concluded that oil market fluctuations exhibit less sensitivity than the clean energy downside risk.

To address gaps in the literature, in this study, we selected the GPR and EUI indices as uncertainty measures (Baker et al., 2016; Caldara and Iacoviello, 2018; Caldara and Iacoviello, 2022; Fig. 1), and considered them with reference to five renewable energy sub-sectors markets (i.e., the NASDAQ OMX Solar index, NASDAQ OMX Wind index, NASDAQ OMX Geothermal index, NASDAQ OMX Full Cell index, and NASDAQ OMX Bio-Clean Fuels). We adopted a powerful new method of convergent cross mapping (CCM), as proposed by Sugihara et al. (2012), to identify the time information relationship between renewable energy and the GPR and EUI. On this basis, this study used the impulse response function to more completely express the meaning contained in the Vector Autoregressive Model (VAR) model, and to provide positive and negative directions, adjustment lag length, stability processes, and other information on the response of renewable energy to significant geopolitical and economic events. In addition, a variance decomposition method was used to accurately analyze the contribution of each structural impact to renewable energy change. The impulse response and variance decomposition methods reasonably identified asymmetric responses in conditional variances and correlations during the COVID-19 pandemic (Ghabri et al., 2021; Lee et al., 2021; Mugaloglu et al., 2021). Furthermore, wavelet coherence methods involving time-varying and depend on time frequency and allowed us to decompose returns series (Hoon et al., 2019; Goodell and Goutte, 2021; Yousfi et al., 2021). Our findings indicate the positive impact of economic uncertainty on clean energy.

The following sections of this paper are organized as follows: section 2 describes the data sources model definitions; section 3 identifies the time information relationship between renewable energy and the GPR and EUI; section 4 investigates the dynamic interaction effects of renewable energy on notable geopolitical and economic events; and section 5 proposes renewable energy as a safe-haven asset. Finally, section 6 concludes and provides policies.

2. Data and model

2.1. Data

As shown in Fig. 2, the GPR and EUI are uncertainty indices collected from the Federal Reserve Bank of St. Louis. The renewable energy indices included five sub-sectors: the NASDAQ OMX Solar index, NASDAQ OMX Wind index, NASDAQ OMX Geothermal index, NASDAQ OMX Full Cell index, and NASDAQ OMX Bio-Clean Fuels index. Data analysis covered the period from March 30, 2012 to April 1, 2022. We measured the performance via realized volatility and introduced a logarithm for better estimation, shown in Eq. (1).

$$RV = \sum_{j=1}^{M} r^2 \quad (1)$$

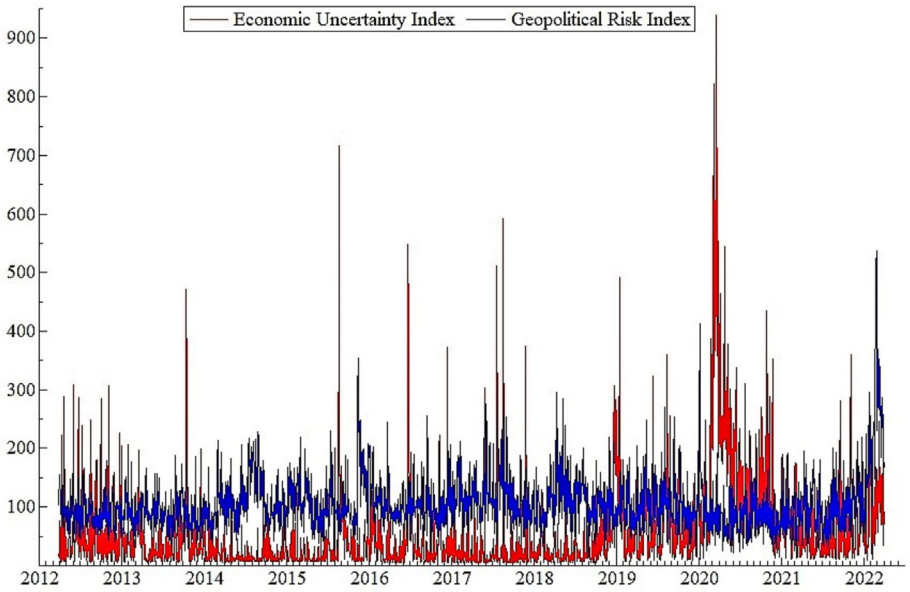

Fig. 1. Geopolitical risk and economic uncertainty indices. The *y*-axis represents the size of geopolitical risk and economic uncertainty indices, which are dimensionless indices without unit. The horizontal *x*-axis represents time.

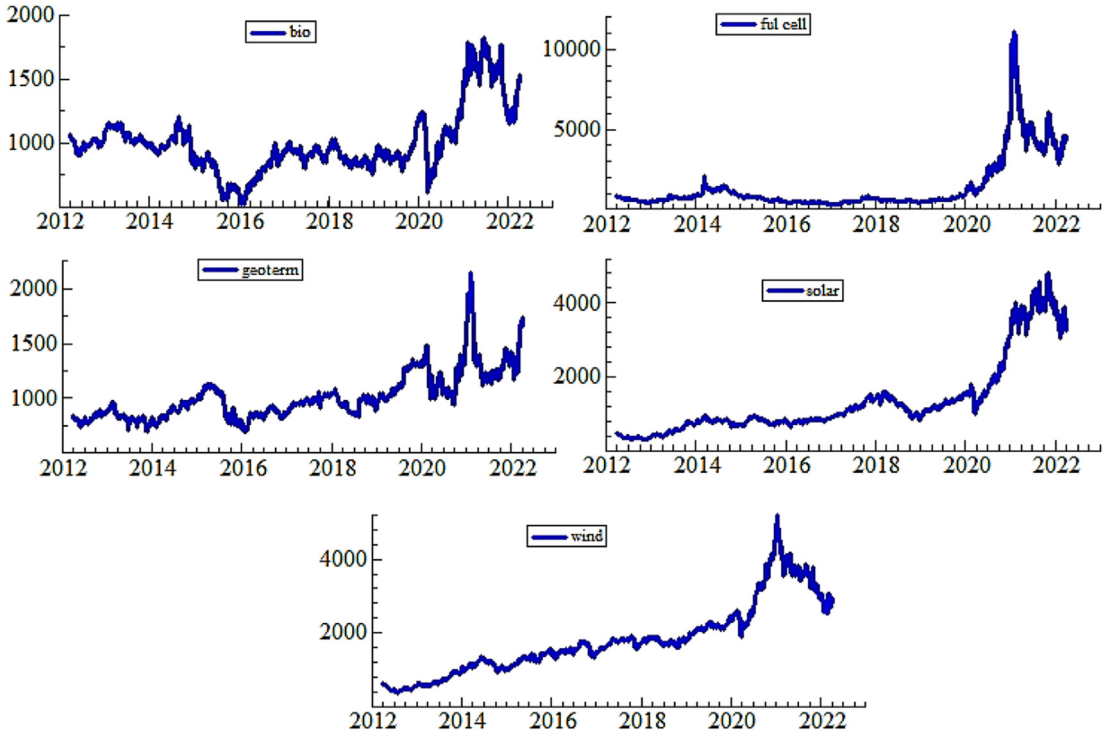

Fig. 2. Price dynamics of renewables indices. The *y*-axis represents the price dynamics of renewables indices, which are dimensionless indices without unit. The horizontal *x*-axis represents time.

where j represents the jth day since day t, M stands for the number of observations on day t, which can be described as shown in Eq. (2).

$$R_{it} = \ln\left(\frac{T_{it}}{T_{t-1}}\right) \tag{2}$$

where T_{it} represents the index at time t, T_{t-1} represents the index at time $t-1$, and R_{it} represents the index return at time t.

2.2. Model definitions

2.2.1. Convergent cross mapping

To detect causal relationships from nonlinear dynamic systems, CCM is based on Taken's theorem and state space reconstruction (Takens, 1981; Deyle and Sugihara, 2011). CCM has been applied in many research fields including ecology, biology, and geography (Wang et al., 2014; Yao, 2017; Ushio et al., 2018).

The choice of two parameters is vital for State Space Reconstruction (SSR): time lag (τ) and embedding dimension (e). Although some scholars argue that the determination of parameters is not sensitive for CCM results (Chen et al., 2017), to guarantee the accuracy of results, average mutual information criterion (AMI) and averaged false neighbors (AFN) method were applied in this study (Kantz and Schreiber, 2004). Following the algorithms of AMI, the mutual information $I(\tau)$ as a function of τ was given. If the time lag is small, $I(\tau)$ will be large, and will decrease more or less rapidly with the decrease of τ. When the first minimum value of $I(\tau)$ appears, the maximal information will be given; that is, the optimal τ is determined. According to the essential theorem of AFN, $E1(e)$ and $E2(e)$ are generated based on the optimal τ. However, it is first necessary to distinguish deterministic data from stochastic data. In principle, for random data, the value of $E1(e)$ will not become saturated as e increases; regardless of the value of e, $E2(e)$ should be equal to 1. In contrast, for deterministic data, the value of $E2(e)$ is not constant and $E1(e)$ should attain a saturated value as e increases, at which point it becomes stable. Optimal e is identified when a value of $E1(e)$ first exceeds the threshold; here, the threshold of $E1(e)$ was set to 0.95 (Cao, 1997). Based on the optimal τ and e, S-maps were applied to test nonlinearity (Sugihara, 1994). For nonlinear systems, predictive skill should decrease as the predictive step increases; this situation is "necessary but insufficient" for nonlinearity.

The CCM method argues that as for any single variable of a multidimensional dynamical system, its time series can include the essential information of the system. For X in dynamical systems, the e time-lagged values (time lags 0, τ, 2τ, …, (e-1) τ) are used as coordinate axes to reconstruct its shadow attractor manifold M_X. M_X is a diffeomorphic reconstruction of the original attractor manifold M. The point on M_X maps 1:1 to the points on M, and the local neighborhoods on M_X map 1:1 to the local neighborhoods on M. According to the SSR is that if the two variables X and Y are dynamically coupled, their shadow attractor manifold M_X and M_Y will map onto each other. If X (cause variable) influences Y (effect variable), the prediction of X can be obtained from the M_Y using a simplex projection; Y cross map X. Analogously, the crossing mapping from X to Y is defined. The Pearson correlation coefficient between prediction and observation of X is regarded as the predictive skill (ρ), which will converge to a peak value with the increase in library length. The value of predictive skill can be viewed as the strength of the causal effect of the X variable on the Y variable. To test the significance of predictive skill, Clark et al. (2015) combined nonparametric bootstrapping technology with CCM. The main principle was to repeat the CCM process for A iterations and count the times B that ρ at the longest library is greater than ρ at the shortest library. The p value can be calculated as (A − B)/A, which represents the probability of rejecting the null hypothesis (i.e., X does not cause Y). In our analysis, the iteration was set to 100. The essential mechanics of multispatial CCM are detailed in Clark et al. (2015).

2.2.2. Generalized impulse response function

The generalized impulse response function (GIRF) was used to further analyze the dynamic interaction of renewable energy with the GPR and EUI. The GIRF measures the dynamic impact of a standard deviation shock from a randomly perturbed term of an endogenous variable on the current and future values of all endogenous variables in the VAR model and this method is widely used in economic analysis (Pesaran and Shin, 1998; Plagborg-Møller and Wolf, 2021). Assuming that the first element of $\boldsymbol{\varepsilon}_t$ changes by δ_1, the second element by δ_2, and the kth element by δ_k, the shock in period t is $\delta = (\delta_1, \delta_2, \ldots, \delta_k)'$. Assuming that $\boldsymbol{\varepsilon}_t$ is a shock of a specific size and occurs only in the jth variable, the response of the vector $\boldsymbol{y}_{t+q}$ to the shock can be expressed as demonstrated in Eq. (3). In Eq. (3), $\boldsymbol{\Omega}_{t-1}$ denotes the set of information in period $t-1$ and m is the prediction level. In order to obtain the results of Eq. (3), it is necessary to first calculate the changes that occur in other elements in $\boldsymbol{\varepsilon}_t$ due to ε_{jt} a shock ε_t at the same time, when $\delta = E(\boldsymbol{\varepsilon}_t|\varepsilon_{jt} = \delta_j)$. Assuming that $\boldsymbol{\varepsilon}_t$ obeys a multivariate normal distribution, δ can be calculated using Eq. (4), where $\sigma_{jj} = E(\varepsilon_{jt}{}^2)$ and $\boldsymbol{\Sigma}_j = E(\boldsymbol{\varepsilon}_t\varepsilon_{jt})$ denotes the jth column of the $\boldsymbol{\varepsilon}_t$ covariance matrix $\boldsymbol{\Sigma}$ element, at which point the response of the vector $\boldsymbol{y}_{t+}$ due to the shock of variable j can be shown in Eq. (5). In Eq. (5), $\boldsymbol{\Theta}_q$ is the coefficient matrix of VAM(q). If we set $\delta = (\sigma_{jj})^{1/2}$, the GIRF is constructed as can be seen in Eqs. (3)–(6).

$$y_{it} = \sum_{j=1}^{k}(\theta_{ij}^{(0)}\varepsilon_{jt} + \theta_{ij}^{(1)}\varepsilon_{jt-1} + \theta_{ij}^{(2)}\varepsilon_{jt-2} + \theta_{ij}^{(3)}\varepsilon_{jt-3} + \ldots) \quad i = 1, 2, \ldots, k, t = 1, 2, \ldots, T \tag{3}$$

$$y_{it} = \sum_{j=1}^{k}(\theta_{ij}^{(0)}\varepsilon_{jt} + \theta_{ij}^{(1)}\varepsilon_{jt-1} + \theta_{ij}^{(2)}\varepsilon_{jt-2} + \theta_{ij}^{(3)}\varepsilon_{jt-3} + \ldots) \quad i = 1, 2, \ldots, k, t = 1, 2, \ldots, T \tag{4}$$

$$y_{it} = \sum_{j=1}^{k}(\theta_{ij}^{(0)}\varepsilon_{jt} + \theta_{ij}^{(1)}\varepsilon_{jt-1} + \theta_{ij}^{(2)}\varepsilon_{jt-2} + \theta_{ij}^{(3)}\varepsilon_{jt-3} + \ldots) \quad i = 1, 2, \ldots, k, t = 1, 2, \ldots, T \tag{5}$$

$$y_{it} = \sum_{j=1}^{k}(\theta_{ij}^{(0)}\varepsilon_{jt} + \theta_{ij}^{(1)}\varepsilon_{jt-1} + \theta_{ij}^{(2)}\varepsilon_{jt-2} + \theta_{ij}^{(3)}\varepsilon_{jt-3} + \ldots) \quad i = 1, 2, \ldots, k, t = 1, 2, \ldots, T \tag{6}$$

2.2.3. Variance decomposition method

The GIRF describes the impact of shocks to one standard variable on the other variables in the VAR model. The importances of different structural impulses are further evaluated using the variance decomposition method, by analyzing the contribution of impulses to each variable, and then on other variables. Thus, the variance decomposition method gives the relative importance information of each random disturbance that affects the variables in the VAR model. In this case, the relative variance contribution was based on the relative contribution of the jth variable's shock-based variance to the variance of y_i to observe the effect of the jth variable on the ith variable. If the model satisfies the smoothness condition, then $\theta_{ij}^{(q)}$ decays geometrically as q increases, and so only a finite number of s terms need to be taken. The Relative Variance Contribution (RVC) is expressed in Eq. (7), where, if $RVC_{j\to i}(s)$ is large, it means that the jth variable has a large effect on the ith variable:

$$RVC_{j\to i}(s) = \frac{\sum_{q=0}^{s-1}(\theta_{jj}^{(q)})^2\sigma_{jj}}{\sum_{j=1}^{k}\left\{\sum_{q=0}^{s-1}(\theta_{jj}^{(q)})^2\sigma_{jj}\right\}}, i,j = 1,2,\ldots k \tag{7}$$

2.2.4. Wavelet coherence

The wavelet coherence equation was:

$$W^2(p,q) = \frac{|M(M^{-1}1N_{ab}(p,q)|^2}{M(M^{-1}|N_a(p,q)|^2 M(M^{-1}|N_b(p,q)|^2} \tag{8}$$

where M is the smoothing operator. The value of wavelet squared coherence ranges from 0 to 1 [$0 \le W^2(p,q) \le 1$]. There is an absence of correlation if wavelet squared coherence is close to 0, and a high correlation when it is close to 1. The wavelet squared coherence is a positive value that cannot distinguish between positive and negative correlation. For this, we used the Monte Carlo method, in which up-right and down-left (↗↙) allow us to ascertain whether the first asset lead a positive correlation or negative correlation, respectively, against the second asset. Down-right and up-left (↘↖) arrows indicate that the second variable leads the first. Up (↑) and down (↓) indicators imply that the variable is leading and lagging, respectively. Wavelet coherency can be indicted by a straight arrow to the right or left (→, ←), indicating that both returns are in phase (positive dependence) or out of phase (negative dependence), respectively. For more details, see Torrence and Compo (1998).

3. Relationship identification results

Table 1 presents the summary statistics of all series returns. All of the series had means that were high and close to 1. The standard deviation was very weak for all renewable energy indices. The standard deviation of the EUI was higher than that of the GPR. The series exhibited excess kurtosis (kurtosis values of ≥3), while the clean energy indices showed less kurtosis than the GPR and EUI. Moreover, the skewness coefficients were not zero, indicating a non-symmetric series. The skewness coefficient of oil prices was negative. The Jarque–Bera test and normality for all the series were significant, meaning the series do not have a normal distribution. Augmented Dickey–Fuller (ADF) and Phillips and Perron (PP) tests for all series revealed stationarity.

Before applying the CCM method, it was necessary to show the mirage correlation of renewable energy with the GPR and EUI pair. The correlation coefficients for the renewable energy markets with the GPR and EUI pair were significant and mostly positive; the absolute values of the correlation coefficients were <0.3, indicating that each renewable energy market with the GPR and EUI pair constitutes a weakly coupled system. As the indispensable basis of the CCM algorithm, SSR depends on two key parameters: time lag (τ) and embedding dimension (e). According to the average mutual information criterion (AMI), the optimal τ is decided by the first minimum of AMI. The optimal τ values to reconstruct the time series of bio-clean fuel, wind, solar, fuel cell, geothermal, GPR, and EUI were 80, 45, 57, 70, 36, 4, and 7, respectively. Based on the optimal τ, the optimal e was determined by the AFN method. When the first value of $E1(e)$ exceeds the threshold and reaches the saturation point, the corresponding e is optimal. In our study, the optimal e values for bio-clean fuel, wind, solar, geothermal, fuel cell, GPR, and EUI were 12, 7, 7, 6, 7, 12 and 11, respectively.

After the determination of parameters and the nonlinearity test, the CCM causal detection approach was applied to identify the effects of renewable energy on the GPR and EUI pair. The convergence of predictive skill is the criterion to judge causality, and the value of predictive skill at the maximum library length [ρ(Lmax)] represents the strength of the causal link. For example, Fig. 3 demonstrates a significance cross map signal between wind and GPR, which indicates a clear asymmetric interaction between wind and GPR; ρ(Lmax) = 0.221 that and the "GPR xmap wind"

Table 1
Descriptive statistics.

	Bio-clean fuels	Solar	Wind	Full cell	Geothermal	GPR	EUI
Mean	0.990	0.990	0.990	0.990	0.990	1.020	1.230
Std Dv	0.005	0.006	0.005	0.010	0.005	0.219	0.943
Skewness	−0.981	−0.429	−0.324	0.512	0.587	2.024	3.252
Kurtosis	16.803	9.514	7.666	7.791	17.171	22.099	21.935
Jarque-Bera	20,966.420	4657.278	2393.376	2589.212	21,810.930	41,118.430	43,240.770
Probability	0.000	0.000	0.000	0.000	0.000	0.000	0.000
ADF	−18.71***	−33.21***	−48.43 ***	−51.4***	−52.82 ***	−36.2***	−37.9***
PP	−53.16***	−40.87 ***	−48.39 ***	−51.4***	−52.83***	−119***	−70.30***
Observations	2589	2589	2589	2589	2589	2589	2589

Note: *** denotes 1% statistical significance level, ** denotes 5% statistical significance level, * denotes 10% statistical significance level.

is lower than ρ(Lmax) = 0.673, the "wind xmap GPR," indicating that the influence of wind on GPR may be lower than that of GPR on wind. There is a clear asymmetric interaction between wind and EUI; ρ(Lmax) = 0.811, the "EUI xmap wind" is slightly lower than ρ(Lmax) = 0.844, the "wind xmap EUI," indicating that the influence of wind on EUI may be lower than that of EUI on wind. Overall, the mean of the predictive skill in the renewable energy xmap EUI (0.602) was lower than the renewable energy xmap GPR (0.803), indicating that the influence of GPR on renewable energy may be greater than that of EUI on renewable energy. The mean predictive skill of EUI xmap renewable energy (0.700) was greater than GPR xmap renewable energy (0.272), indicating that the influence of renewable energy on EUI may be greater than renewable energy on GPR.

The other renewable energy indices also have relationships with GPR and EUI. However, while this shows that renewable energy can be affected by GPR and EUI, the positive or negative impact identified by the CCM approach may be spurious.

4. Dynamic interaction effects

CCM was used to establish the associations between renewable energy and GPR/EUI; however, this approach could not account for the direction, lag length, impact level, or contribution rate of the impulse. In this section, the responses to five sub-sectors of renewable energy utilizing the impulse response method and variance decomposition approach were further addressed. These variables were modeled in this study using a VAR framework with a maximum lag set at 500. The optimal lag was determined according to the minimization principle in accordance with the HQ criterion.

Table 2 shows the response of the bio-clean fuels index after being subjected to an external impulse. For a standard deviation information impulse from the GPR, the bio-clean fuels index initial response velocity was 20.14 in the positive direction with a lag length of 2; the response curve showed an increasing trend followed by a decreasing trend, and reached the highest point at a lag length of 24. For a standard information impulse from the EUI, the bio-clean fuels index initial response rate was 50.15 with a lag length of 2; the response curve showed a decreasing and then increasing trend and reached the lowest point at a lag length of 79. In terms of the cumulative effect, the GPR produced a positive impact on the bio-clean fuels index, while the EUI produced a negative impact; and GPR produced a higher impact than EUI. In addition, the bio-clean fuels index had a positive response to the bio-clean fuels index in the first 100 lag lengths, while the EUI had a negative response to the bio-clean fuels index. The bio-clean fuels index responded significantly faster to both in the first 100 lag lengths than in the latter. After the GPR and EUI impulse, the adjustment time of the renewable energy index was ∼90 lag lengths, and the response curve eventually flattened out. According to the results of variance decomposition, the bio-clean fuels index was dominant despite its decreasing contribution to its own change. GPR had a higher contribution than EUI, and both showed an increasing trend. The contribution rate tended to stabilize at ∼60 lag lengths, indicating that GPR has a higher degree of influence on the bio-clean fuels index than does EUI, which is consistent with the results of impulse response.

Table 3 shows the response of the wind index after being subjected to external impulses. For a standard deviation information impulse from the GPR, the initial response speed of the wind index was 1.20 in the positive direction with a lag length of 2, and the response curve showed a decreasing and then increasing trend, reaching the highest point at a lag length of 135. For a standard information impulse from the EUI, the initial response rate of the wind index was 50.15 with a lag length of 2; the response curve tended to rise and then fall, reaching the lowest point at a lag length of 108. In terms of the cumulative effect, GPR produced a negative effect on the wind index; EUI had a positive effect on the bio-clean fuels index and GPR produced a much lower impact than EUI, which is the opposite of the response direction exhibited by the bio-clean fuels index. According to the results of variance decomposition, the contribution of the wind index to its own change has been decreasing but has been in the dominant position. GPR made a higher contribution than EUI, and both showed an increasing trend, which indicates that GPR has a higher degree of influence on the wind index than does EUI.

Table 4 shows the response of the solar index after being subjected to external impulses. For a standard deviation information impulse from the GPR, the solar index initially responded with a positive velocity of 0.67 at a lag length of 2. The response curve showed an increasing followed by a decreasing trend and reached its highest point at a lag length of 6. With time, the response curve gradually decreased and became negative at a lag length of 23. For a standard information impulse from the EUI, the solar index initial response rate was negative (−0.57) at a lag length of 2. The response curve showed a gradual expansion trend; after reaching a lag length of 80, the response rate gradually tended to be stable. In terms of the cumulative impact, GPR had a negative impact on the solar index, while EUI had a positive impact; EUI had a more rapid impact than GPR. In addition, the speed of the bio-clean fuels index in the first 80 lag lengths was significantly higher than that of the latter. According to the results of the variance decomposition, the solar index was in a dominant position, although its contribution to its own change decreased. EUI has a higher contribution than GPR, and both showed an increasing trend. EUI had a higher degree of influence on the solar index than GPR.

Table 5 reflects the response of the full cell index after being subjected to an external impulse. For one standard deviation information impulse from the GPR and EUI, the initial response of the full cell index was 14.69 and 14.82, respectively, at a lag length of 2; it showed an increasing and then decreasing trend, and reached the highest point at lag lengths of 32 and 43, respectively. The two response curves showed obvious consistency; however,

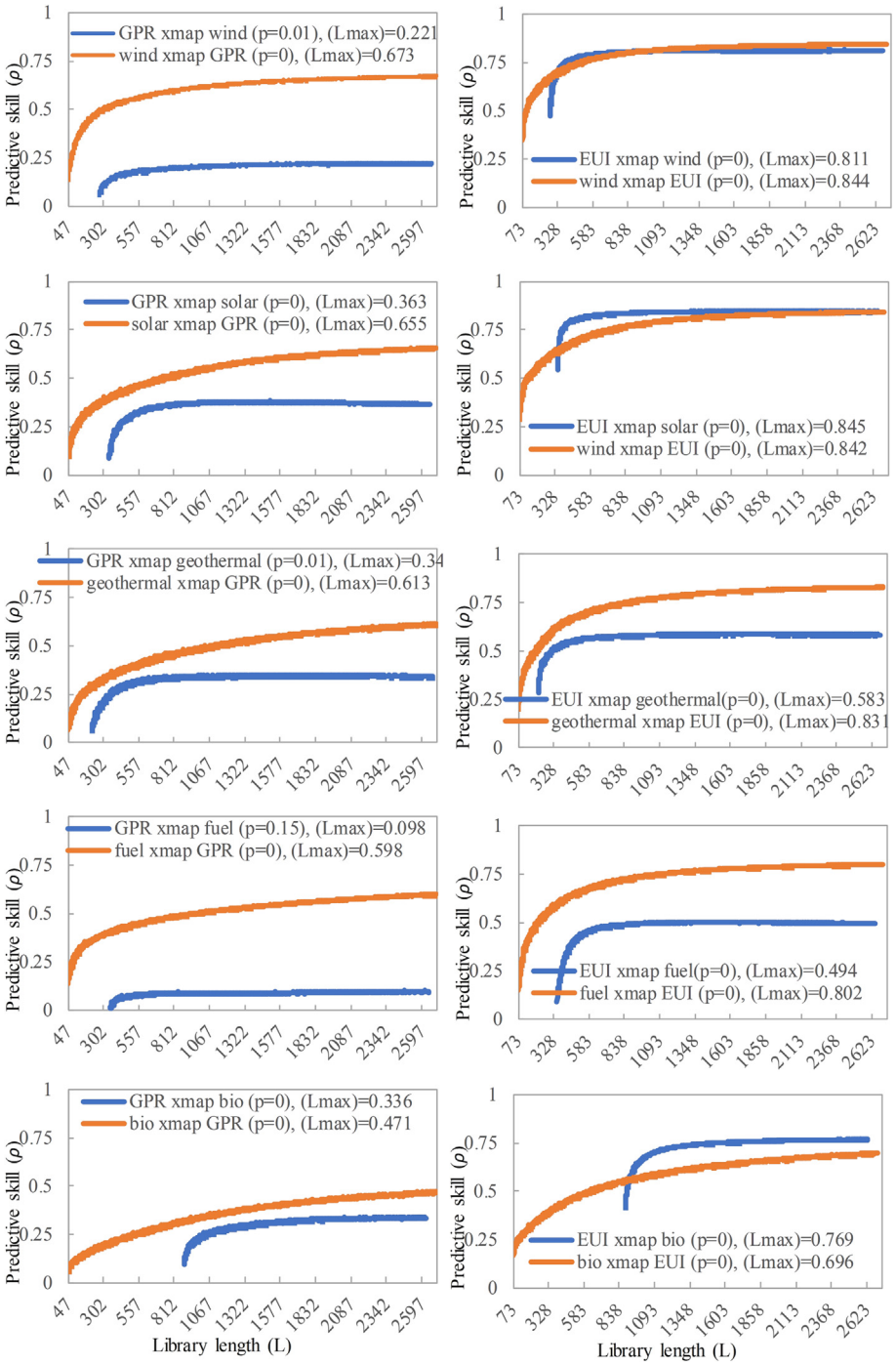

Fig. 3. Effect of renewable energy with the GPR and the EUI. The *y*-axis represents predictive skill, which are dimensionless indices without unit. The horizontal *x*-axis represents library length.

the highest points were 34.13 and 16.82, indicating that the full cell index responds differently to different impulses. These results show that GPR and EUI have positive impacts on the full cell index; GPR generates a higher impact than EUI. The full cell index had a long adjustment time after impulses from the GPR and the EUI, taking ~250 lag lengths to reach 0. According to the variance, the contribution of GPR is higher than that of EUI, both of which showed an increasing trend and stabilized at ~80 lag lengths.

Table 6 shows the response of the geothermal index after being subjected to external impulses. For a standard deviation information impulse from the GPR and EUI, the initial response velocity of the geothermal index was 0.19 and −0.56 at a lag length of 2, respectively; the curves were similar and both showed a rising and then decreasing trend. For the GPR impulse, the response curve reached a maximum of 6.22 at a lag length of 30; for the EUI impulse, the response curve reached the maximum at a lag length of 64. The response time of the geothermal index for the EUI impulse was longer than that of the GPR impulse. These results show that the initial impact on the geothermal index of GPR and EUI is different, and GPR generates a lower effect than EUI. EUI started to generate a positive effect after 3 lag lengths while GPR always had a positive effect. According to the variance decomposi-

Table 2
Impulse response and variance decomposition results of the bio clean fuels.

Lag length	Impulse response		Variance decomposition		
	GPR	EUI	Bio-clean fuels (%)	GPR (%)	EUI (%)
1	0.000	0.000	100.000	0.000	0.000
50	48.583	−6.756	99.001	0.935	0.064
100	24.939	−8.770	98.771	1.153	0.076
150	12.137	−5.407	98.712	1.201	0.087
200	5.841	−2.844	98.697	1.212	0.091
250	2.798	−1.414	98.694	1.215	0.092
300	1.338	−0.687	98.693	1.215	0.092
350	0.639	−0.331	98.693	1.215	0.092
400	0.305	−0.158	98.692	1.215	0.092
450	0.146	−0.076	98.692	1.215	0.092
500	0.070	−0.036	98.692	1.215	0.092

Table 3
Impulse response and variance decomposition results of the wind.

Lag length	Impulse response		Variance decomposition		
	GPR	EUI	Wind (%)	GPR (%)	EUI (%)
1	0.000	0.000	100.000	0.000	0.000
50	−0.975	16.567	89.349	0.083	10.568
100	−1.758	18.470	82.445	0.127	17.428
150	−1.816	18.011	79.248	0.172	20.580
200	−1.750	17.185	77.573	0.197	22.230
250	−1.666	16.332	76.574	0.213	23.213
300	−1.583	15.510	75.919	0.224	23.858
350	−1.503	14.728	75.459	0.231	24.310
400	−1.427	13.984	75.120	0.236	24.644
450	−1.355	13.279	74.861	0.240	24.899
500	−1.287	12.609	74.658	0.244	25.099

Table 4
Impulse response and variance decomposition results of the solar.

Lag length	Impulse response		Variance decomposition		
	GPR	EUI	Solar (%)	GPR (%)	EUI (%)
1	0.000	0.000	100.000	0.000	0.000
50	−1.445	12.550	95.687	0.059	4.255
100	−2.424	15.819	91.537	0.154	8.309
150	−2.672	16.640	89.204	0.228	10.567
200	−2.734	16.843	87.867	0.274	11.859
250	−2.749	16.890	87.036	0.304	12.660
300	−2.752	16.897	86.479	0.323	13.198
350	−2.752	16.894	86.082	0.337	13.581
400	−2.751	16.888	85.786	0.348	13.867
450	−2.750	16.882	85.556	0.356	14.088
500	−2.749	16.876	85.372	0.362	14.265

Table 5
Impulse response and variance decomposition results of the full cell.

Lag length	Impulse response		Variance decomposition		
	GPR	EUI	Full cell (%)	GPR (%)	EUI (%)
1	0.000	0.000	100.000	0.000	0.000
50	31.737	16.701	98.986	0.811	0.203
100	20.902	13.031	98.666	1.037	0.297
150	13.464	8.950	98.568	1.096	0.336
200	8.706	5.922	98.531	1.117	0.352
250	5.639	3.868	98.516	1.125	0.359
300	3.655	2.514	98.510	1.128	0.362
350	2.369	1.632	98.508	1.129	0.363
400	1.536	1.058	98.507	1.130	0.364
450	0.996	0.686	98.506	1.130	0.364
500	0.646	0.445	98.506	1.130	0.364

Table 6
Impulse response and variance decomposition results of the geothermal.

Lag length	Impulse response		Variance decomposition		
	GPR	EUI	Geothermal (%)	GPR (%)	EUI (%)
1	0.000	0.000	100.000	0.000	0.000
50	5.748	5.856	87.665	7.453	4.882
100	4.361	5.595	83.721	8.198	8.081
150	3.444	4.656	82.202	8.270	9.529
200	2.755	3.770	81.475	8.281	10.244
250	2.212	3.035	81.086	8.284	10.630
300	1.776	2.439	80.862	8.285	10.853
350	1.427	1.960	80.728	8.285	10.987
400	1.146	1.574	80.645	8.286	11.069
450	0.921	1.265	80.593	8.286	11.121
500	0.740	1.016	80.560	8.286	11.154

tion, the contribution of the geothermal index to its own change was decreasing, but was always dominant. Before 104 lag lengths, GPR had a higher contribution than EUI; after 104 lag lengths, EUI had a higher contribution than GPR. The contributions of both showed increasing trends.

5. Renewable energy as a safe-haven asset

Fig. 4 shows the time-varying correlation of each renewable energy market with GPR and EUI. Volatility fluctuated between positive and negative change. The dynamic conditional variable increased slightly between each renewable energy and EUI couple during the first (early 2020 to September 2020) and second (February 2021) waves of COVID-19; that is, the COVID-19 pandemic had a positive impact on renewable energy markets. However, between these two periods the impact decreased. The impact of COVID-19 decreased slightly during the Russia–Ukraine conflict, showing that the financial returns of renewable energy decrease when risk increases. These results, along with weak volatile spillover change, confirm that renewable energy sectors can be an opportunity for

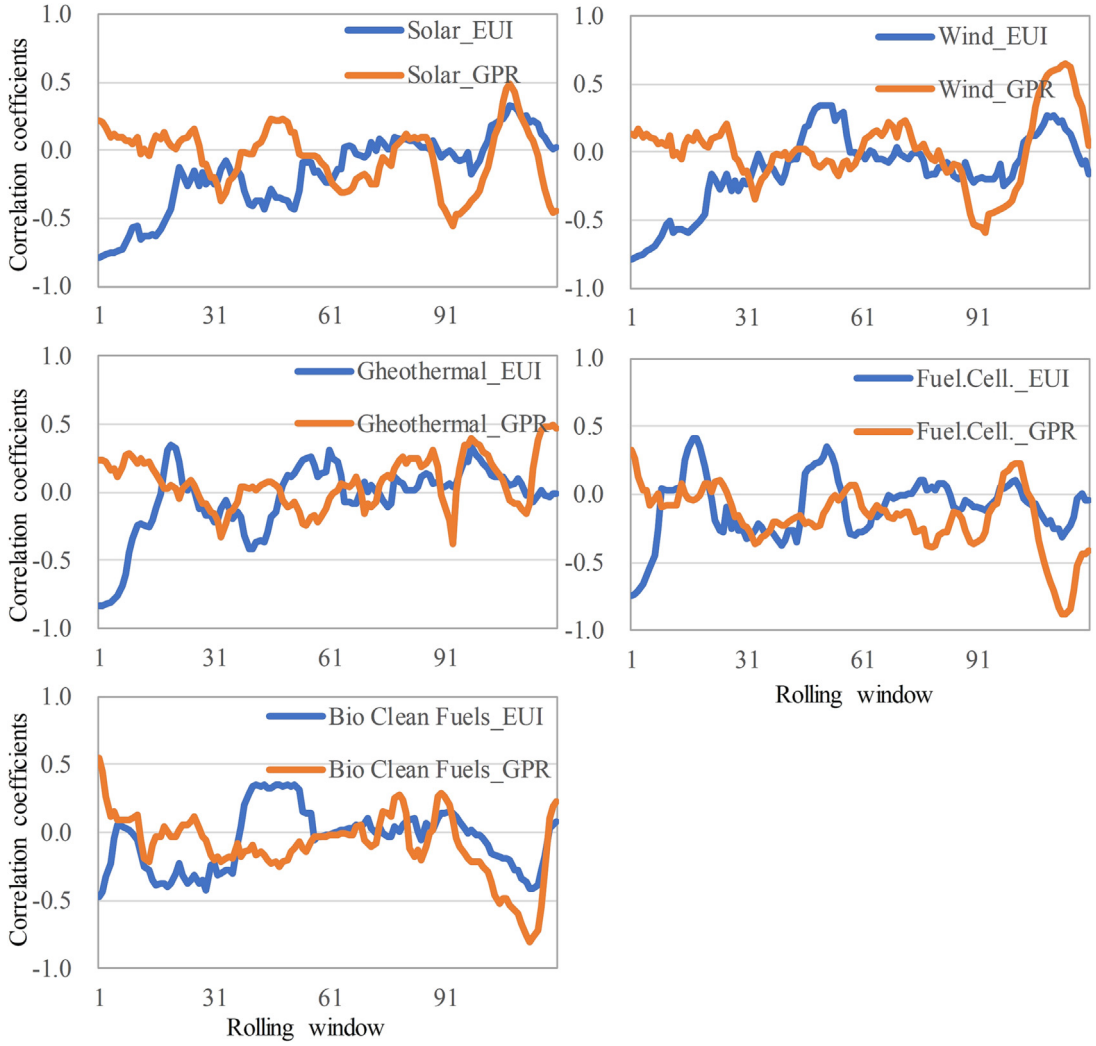

Fig. 4. Correlation coefficients calculating with rolling window. The data are the results of rolling window correlation coefficients calculated for a period starting in 2020, with the window length set to 100 days and the window width set to 5 days.

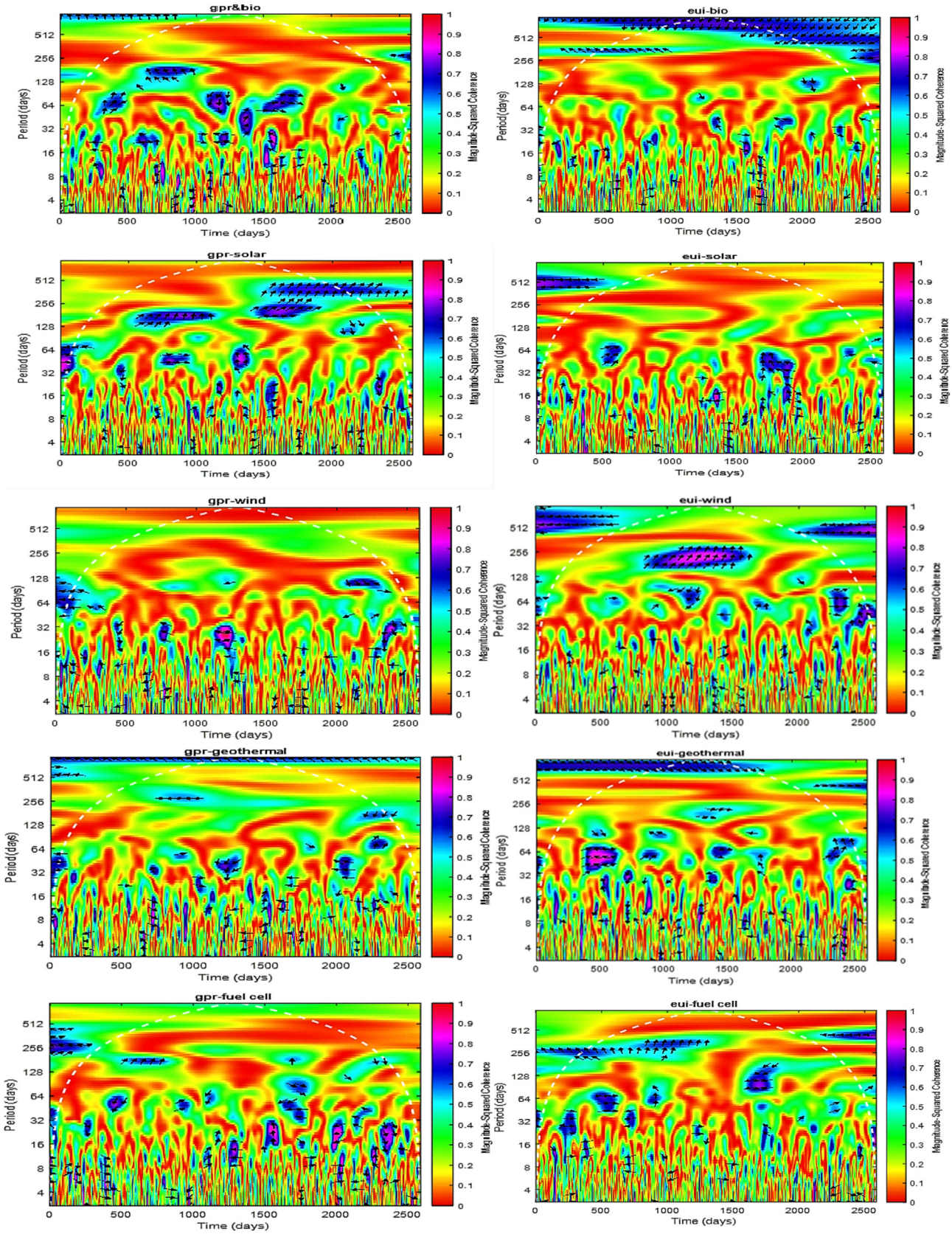

Fig. 5. Wavelets coherence results. To designate the dependence degree, purple (high dependence) to red (less dependence) colors show the degree of co-movement. In addition, the islands or areas inside the wavelet coherence map indicate co-movement between variables. (For interpretation of the references to colour in this figure legend, the reader is referred to the web version of this article.)

portfolio investors during times of geopolitical and economic upheaval. In summary, renewable energy can serve as a safe-haven against economic uncertainty and geopolitical risk under different market conditions (bearish, normal, and bullish).

Fig. 5 shows the coherence of clean energy with GPR and EUI from March 30, 2012 to April 1, 2022. The wavelet coherence trace reveals co-movement at each time and scale between renewable energy and economic and geopolitical risks. The inverted (U) indicates regions with significance at the 5% level.

We identified small areas between the solar index and GPR at a large scale during the Russia–Ukraine conflict (2014) and China–USA trade conflict. The EUI effect showed the weakest connection (and a small island) for the wind index. This explains why the wind and solar indices can act as a soft safe-haven asset against EUI and GPR. Moreover, these results are consistent with past studies (Ahmad et al., 2018; Ji et al., 2018). In the remaining cases, we observed typical first-time phases of small islands and an absence of strong dependence at different scales and times. Notably, risk reduction via weak co-movement between each renewable energy index and GPR or EUI confirmed the safe-haven characteristic of renewable energy during economic and geopolitical turmoil. In summary, renewable energy plays a vital role in international peace, economic stability, and energy security, strengthening the argument for a renewable energy transition.

6. Conclusion and perspectives

In this study, we used the GPR and EUI as uncertainty measures in CCM, GIRF, variance decomposition, wavelet coherence, and other analysis methods, and identified their relationships with a set of renewable energy indices from the NASDAQ. The CCM results show that the renewable energy indices display clear relationships with GPR and EUI. The impulse response results show that for a standard deviation information impulse from the GPR, the response directions of the bio-clean fuels index, full cell index, and geothermal index are positive, while the solar index and wind index have a negative response and differential evolutionary trend. Comparing standard information difference impulses from GPR and EUI, the bio-clean fuels index, wind index, and solar index exhibit opposite responses directions and speeds. The renewable energy indices have short adjustment times after an impulse, taking 60–100 lag lengths to level off, while the solar index and the full cell index take longer to adjust. The results of variance decomposition show that EUI contributes more to the wind index, solar index, and geothermal index than GPR. The impact of the EUI on renewable energy is relatively more important than that of GPR. The dynamic conditional variable increased slightly between each renewable energy and EUI during the first (early 2020 to September 2020) and second (February 2021) waves of COVID-19. Moreover, renewable energy offered a safe-haven investment during the Russia–Ukraine conflict (2022).

Replacing fossil energy with renewable energy is widely supported as a means to tackle global climate change. In recent years, several countries have made significant efforts to develop renewable energy technology, and renewable energy portfolios are rapidly replacing fossil fuel restrictions. As such, the renewable energy industry is poised for greater growth. However, in the context of economic globalization, political and economic uncertainty can impact renewable energy indices, and the development of the renewable energy industry may also face adverse effects owing to short-term cost increases and supply chain bottlenecks. Our study shows that renewable energy development can also significantly increase the energy independence of consuming countries and can drive profound changes in geopolitical situations, reducing the negative effects of political and economic uncertainty. Finally, investing in global renewable energy indices may lower financial risks and increase avenues for profitable investments.

However, in the short term, in addition to the pressure to reduce costs and improved economic efficiency, the large-scale use of renewable energy will require technological breakthroughs. In the current economic environment and at this technological level, it is still difficult for renewable energy to become the dominant form of energy in the international energy market. Individual countries have less need for concern over the negative impacts of political and economic uncertainty, but it is important to be alert to such impacts. In the long run, the future construction of more secure renewable energy systems and the exploration of how to use renewable energy as a risk-averse tool needs to be considered. From a research perspective, we plan to quantify renewable energy risk using inter-day data, which will reveal high-frequency volatility. Moreover, we plan to compare property investments against financial assets such as Bitcoin, gold, oil, and stock markets.

CRediT authorship contribution statement

Xin Zhao: Conceptualization, Writing – original draft, Writing – review & editing. **Kamel Si Mohammed:** Methodology, Visualization. **Yaohui Wang:** Conceptualization, Software, Visualization, Writing – review & editing. **Paweł Stępień:** Writing – review & editing, Supervision. **Grzegorz Mentel:** Software, Writing – review & editing.

Declaration of Competing Interest

The authors declare that they have no known competing financial interests or personal relationships that could have appeared to influence the work reported in this paper.

Acknowledgements

This work was supported by the Ministry of Education of the People's Republic of China Humanities and Social Sciences Youth Foundation (Grant No. 22YJC910014), the Social Sciences Planning Youth Project of Anhui Province (Grant No. AHSKQ2022D138), the Anhui Province Excellent Young Talents Fund Program of Higher Education Institutions (Grant No. 2023AH030015), and the Innovation Development Research Project of Anhui Province (Grant No. 2023CX507), and the National Natural Science Foundation of China (Grant No. 71934001).

References

Ahmad, W., Sadorsky, P., Sharma, A., 2018. Optimal hedge ratios for clean energy equities. Econ. Model. 72, 278–295.
Alqahtani, A., Klein, T., 2021. Oil price changes, uncertainty, and geopolitical risks: On the resilience of GCC countries to global tensions. Energy 236, 121541.
Are, E., Di, T., Liu, T., Hamori, S., 2020. Spillovers to renewable energy stocks in the US and Europe: Are they different? Energies 13, 1–28.
Azad, N.F., Serletis, A., 2021. Spillovers of U.S. monetary policy uncertainty on inflation targeting emerging economies. Emerg. Mark. Rev. 51, 100875.
Bai, X., 2021. Tanker freight rates and economic policy uncertainty: A wavelet-based copula approach. Energy 235, 121383.
Baker, S.R., Bloom, N., Davis, S.J., 2016. Measuring economic policy uncertainty. Q. J. Econ. 131, 1593–1636.
Caldara, D., Iacoviello, M., 2018. Measuring geopolitical risk. International Financ Discussion Papers 1222, 1–66 https://doi.org/10.17016/IFDP.2018.1222r1.
Caldara, D., Iacoviello, M., 2022. Measuring Geopolitical Risk. Am. Econ. Rev. 114, 1194–1225.
Cao, L., 1997. Practical method for determining the minimum embedding dimension of a scalar time series. Physica D: Nonlinear Phenomena 110, 43–50.
Chen, Z., Cai, J., Gao, B., Xu, B., Dai, S., He, B., Xie, X., 2017. Detecting the causality influence of individual meteorological factors on local $PM_{2.5}$ concentration in the Jing-Jin-Ji region. Scientific Reports 7 (1), 40735.
Chen, Y., Zhu, X., Li, H., 2022. The asymmetric effects of oil price shocks and uncertainty on non-ferrous metal market: Based on quantile regression. Energy 246, 123365.

Clark, A.T., Ye, H., Isbell, F., Deyle, E.R., Cowles, J., Tilman, G.D., Sugihara, G., 2015. Spatial convergent cross mapping to detect causal relationships from short time series. Ecology 96, 1174–1181.
Davidescu, A.A., Apostu, S.A., Stoica, L.A., 2021. Socioeconomic effects of Covid-19 pandemic: Exploring uncertainty in the forecast of the romanian unemployment rate for the period 2020–2023. Sustainability 13 (13), 7078.
Deyle, E.R., Sugihara, G., 2011. Generalized theorems for nonlinear state space reconstruction. Plos One 6 (3), e18295.
Dibiasi, A., Abberger, K., Siegenthaler, M., Sturm, J.E., 2018. The effects of policy uncertainty on investment: Evidence from the unexpected acceptance of a far-reaching referendum in Switzerland. Eur. Econ. Rev. 104, 38–67.
Diebold, F.X., Yilmaz, K., 2014. On the network topology of variance decompositions: Measuring the connectedness of financial firms. J. Econom. 182, 119–134.
Dutta, A., 2017. Oil price uncertainty and clean energy stock returns: New evidence from crude oil volatility index. J. Clean. Prod. 164, 1157–1166.
Eksi, O., Tas, B.K.O., 2022. Time-varying effect of uncertainty shocks on unemployment. Econ. Model. 110, 105810.
Ghabri, Y., Ayadi, A., Guesmi, K., 2021. Fossil energy and clean energy stock markets under COVID-19 pandemic. Appl. Econ. 53, 4962–4974.
Goodell, J.W., Goutte, S., 2021. Co-movement of COVID-19 and Bitcoin: Evidence from wavelet coherence analysis. Finance Res. Lett. 38, 101625.
Gozgor, G., Lau, M.C.K., Zeng, Y., Yan, C., Lin, Z., 2022. The impact of geopolitical risks on tourism supply in developing economies: The moderating role of social globalization. J. Travel Res. 61, 872–886.
Hemrit, W., Benlagha, N., 2021. Does renewable energy index respond to the pandemic uncertainty? Renew. Energy 177, 336–347.
Hoon, S., Mciver, R.P., Arreola, J., 2019. Co-movements between Bitcoin and Gold: A wavelet coherence analysis. Physica A: Statistical Mechanics and its Applications 536, 120888.
Ji, Q., Liu, B., Nehler, H., Uddin, G.S., 2018. Uncertainties and extreme risk spillover in the energy markets: A time-varying copula-based CoVaR approach. Energy Econ. 76, 115-126.
Jiao, Y., Xiao, X., Bao, X., 2022. Economic policy uncertainty, geopolitical risks, energy output and ecological footprint — Empirical evidence from China. Energy Reports. 8, 324–334.
Johnston, A., 2020. The impacts of the Covid-19 crisis on global energy demand and CO_2 emissions. Global Energy Review. www.iea.org/corrigenda.
Kang, H., An, J., Kim, H., Ji, C., Hong, T., Lee, S., 2021. Changes in energy consumption according to building use type under COVID-19 pandemic in South Korea. Renew. Sustain. Energy Rev. 148, 111294.
Kantz, H., Schreiber, T., 2004. Nonlinear Time Series Analysis. Cambridge University Press, Cambridge.
Lee, C.C., Lee, C.C., Wu, Y., 2021. The impact of COVID-19 pandemic on hospitality stock returns in China. International Journal of Finance & Economics 28 (2), 1787–1800.
Liu, T., Nakajima, T., Hamori, S., 2022. The impact of economic uncertainty caused by COVID- 19 on renewable energy stocks. Empir. Econ. 62, 1495–1515.
Mugaloglu, E., Polat, A.Y., Tekin, H., Kılıç, E., 2021. Assessing the impact of Covid-19 pandemic in Turkey with a novel economic uncertainty index. J. Econ. Stud. 38, 101625.
Overland, I., 2019. The geopolitics of renewable energy: Debunking four emerging myths. Energy Res. Soc. Sci. 49, 36–40.
Pesaran, H.H., Shin, Y., 1998. Generalized impulse response analysis in linear multivariate models. Economics Letters 58, 17–29.
Plagborg-Møller, M., Wolf, C.K., 2021. Local projections and VARs estimate the same impulse responses. Econometrica 89, 955–980.
Su, C.W., Khan, K., Tao, R., Umar, M., 2020. A review of resource curse burden on inflation in Venezuela. Energy 204, 117925.
Sugihara, G., 1994. Nonlinear forecasting for the classification of natural time series. Philosophical Transactions of the Royal Society of London. Series A: Physical and Engineering Sciences. 348 (1688), 477–495.
Sugihara, G., May, R., Ye, H., Hsieh, C.H., Deyle, E., Fogarty, M., Munch, S., 2012. Detecting causality in complex ecosystems. Science 338, 496–500.
Sweidan, O.D., 2021. The geopolitical risk effect on the US renewable energy deployment. J. Clean. Prod. 293, 126189.
Takens, F., 1981. Detecting strange attractors in turbulence. Paper presented at the Dynamical Systems and Turbulence, Warwick 1980, Berlin, Heidelberg.
Tiwari, A.K., Das, D., Dutta, A., 2019. Geopolitical risk, economic policy uncertainty and tourist arrivals: Evidence from a developing country. Tour. Manag. 75, 323–327.
Tiwari, A.K., Boachie, M.K., Suleman, M.T., Gupta, R., 2021. Structure dependence between oil and agricultural commodities returns: The role of geopolitical risks. Energy 219, 119584.
Torrence, C., Compo, G.P., 1998. A practical guide to wavelet analysis. Bull. Am. Meteorol. Soc. 79, 61–78.
Ushio, M., Hsieh, C.H., Masuda, R., Deyle, E.R., Ye, H., Chang, C.W., Sugihara, G., Kondoh, M., 2018. Fluctuating interaction network and time-varying stability of a natural fish community. Nature 554, 360–363.
Vakulchuk, R., Overland, I., Scholten, D., 2020. Renewable energy and geopolitics: A review. Renew. Sustain. Energy Rev. 122, 109547.
Wang, X., Piao, S., Ciais, P., Friedlingstein, P., Myneni, R.B., Cox, P., Heimann, M., Miller, J., Peng, S., Wang, T., Yang, H., Chen, A., 2014. A two-fold increase of carbon cycle sensitivity to tropical temperature variations. Nature 506, 212–215.
Xue, C., Shahbaz, M., Ahmed, Z., Ahmad, M., Sinha, A., 2022. Clean energy consumption, economic growth, and environmental sustainability: What is the role of economic policy uncertainty? Renew. Energy 184, 899–907.
Yahya, M., Kanjilal, K., Dutta, A., Uddin, G.S., Ghosh, S., 2021. Can clean energy stock price rule oil price? New evidences from a regime-switching model at first and second moments. Energy Econ. 95, 105116.
Yang, K., Wei, Y., Li, S., He, J., 2021. Geopolitical risk and renewable energy stock markets: An insight from multiscale dynamic risk spillover. J. Clean. Prod. 279, 123429.
Yao, L., 2017. Causative impact of air pollution on evapotranspiration in the North China Plain. Environ. Res. 158, 436–442.
Yousfi, M., Ben Zaied, Y., Ben Cheikh, N., Ben Lahouel, B., Bouzgarrou, H., 2021. Effects of the COVID-19 pandemic on the US stock market and uncertainty: A comparative assessment between the first and second waves. Technol. Forecast. Soc. Change 167, 120710.